



# Experimental investigation of mechanical properties and energy absorption capabilities of hybrid lattice structures manufactured using fused filament fabrication

Daniyar Syrlybayev<sup>1</sup> · Asma Perveen<sup>1</sup> · Didier Talamona<sup>1</sup>

Received: 14 September 2022 / Accepted: 14 January 2023 / Published online: 27 January 2023  
© The Author(s) 2023

## Abstract

Hybrid lattice structures are composed of several dissimilar unit cells arranged in specific patterns. Unlike their one-phase counterparts, hybrid lattices remain relatively unexplored. In this work, novel hybrid lattice structures composed of Pillar Octahedral (PO) and Rhombic Dodecahedron (RD) lattices having variable strut diameters are arranged in different orders to form hybrid vertical piles (HVP), 2D and 3D chessboard order (HCh2D and HCh3D), are proposed, and their mechanical properties, energy absorption characteristics, and deformation modes are investigated under quasistatic compression. The empirical results indicated that the mechanical properties of hybrid lattice structures are the average of those of their parent lattices. HVP lattice structure has a high yield stress of 1.2, 2.22, and 3.54 MPa when strut diameter is 1.5, 1.75, and 2 mm respectively, and stable post-buckling region. It was also observed that hybrid lattice structures are more efficient in absorbing the energy of the deformation. When strut diameter is 1.5 mm, PO lattice structure has an efficiency of 50%, while HVP, HCh2D, and HCh3D lattices have an efficiency of about 70–80%. Finally, Gibson-Ashby models were proposed to predict the mechanical properties of lattice structures as the function of relative density.

**Keywords** Hybrid lattice structures · Fused filament fabrication · Polymeric material · Quasi-static compression

## Abbreviations

AM	Additive manufacturing
BCC	Body-centered cubic lattice
BCCZ	Body-centered cubic lattice with vertical pillar
FCC	Face-centered cubic lattice
FCCZ	Face-centered cubic lattice with vertical pillar
FFF	Fused filament fabrication
HCh2D	Hybrid 2-dimensional Chessboard arrangement
HCh3D	Hybrid 3-dimensional Chessboard arrangement
HVP	Hybrid vertical pile arrangement
PLA	Polylactic acid
PO	Pillar octahedral
PVA	Polyvinyl alcohol
RD	Rhombic dodecahedron
TPMS	Triply periodic minimal surface

## Nomenclature

$E_s$	Elastic modulus of the solid parent material
$\varepsilon_d$	Densification strain
$\sigma_p$	Plateau stress of the lattice structure
$\sigma_y$	Yield stress of the lattice structure
$\sigma_{ys}$	Yield stress of the parent material
$A$	Initial cross-sectional area of the lattice bounding box
$E$	Elastic modulus of the lattice structure
$F$	Force
$h$	Lattice height
$\delta$	Deformation of the lattice
$\varepsilon$	Strain
$\eta(\varepsilon)$	Energy absorption efficiency at strain $\varepsilon$
$\rho/\rho_s$	Relative density
$\sigma$	Stress
$\psi(\varepsilon)$	Volumetric energy absorption at strain $\varepsilon$
$SEA(\varepsilon)$	Specific energy absorption at strain $\varepsilon$

✉ Didier Talamona  
didier.talamona@nu.edu.kz

<sup>1</sup> Mechanical and Aerospace Engineering Department, School of Engineering and Digital Sciences, Nazarbayev University, 53 Kabanbay Batyr Ave., Astana 010000, Kazakhstan

## 1 Introduction

Lattice structures belong to the special class of porous materials, which have a periodically ordered structure. Unlike stochastic porous materials, the geometry of the lattice structure is determined by the unit cell which is repetitively arranged in all coordinate directions. Thus, the properties of lattice structures are determined by the strut geometry (length and diameter) and connectivity (topology), and by controlling these parameters, the properties of lattice structures can be controlled [1]. In addition, unlike solid materials, lattice structures are not occupying the entire bounding box, but leave pores, which reduces the mass of the structure. By varying the strut length and diameter to control the porosity, it is possible to achieve weight reductions of the structure of up to 90–95% compared to the bulk material [2, 3].

These advantages recently expanded the applications of lattice structures and now they are used in advanced fields like aerospace, automotive, and biomedical. In biomedical engineering, lattice structures with tailored mechanical properties are used for the manufacturing of the porous implants [4–9]. By controlling the mechanical properties, it is possible to customize the stiffness of the implant, which may be equal to that of the bone, and avoid stress shielding [5]. In addition, low mass and high strength-to-weight ratio allow the lattice structures to be used in aerospace. For example, Anisogrid composite lattice structures have been used in load-carrying structures to prevent bending and buckling [10, 11]. The reduced mass of the lattice structure has been used to increase the payload of rockets. Finally, lattice structures found their applications in the automotive industry [12] in the design of the optimized structures with the high load carrying capacity [13].

Despite the numerous advantages and applications of lattice structures, their manufacturing using conventional methods is complicated due to the intricate geometry of the parts. In one of the recent studies, it was found that vacuum-assisted rapid investment leads to multiple defects such as incomplete filling and premature solidification of several lattice topologies [14]. As a result, additive manufacturing (AM) remains the main method to produce lattice structures. Compared to conventional manufacturing methods, AM has the advantage of producing parts of complex geometry. This is achieved by slicing the part into thin 2D layers and building each layer on top of the other. In metal powder-based AM technologies, the part is built by melting or sintering the powder, while in polymer filament-based fused filament fabrication (FFF), this is done by depositing molten filament [15]. These two methods remain the most popular for the production of polymer and metallic lattice structures.

With the recent development of AM technologies, research on lattice structure surged rapidly. Most of the

research focuses on the investigation of novel lattice structure topologies, their mechanical properties, and their applications. Cell topology is the most crucial factor affecting the mechanical properties and deformation mode. Different topologies under compression loading produce two main deformation modes: stretch-dominated and bending-dominated. In stretch-dominated lattice structures, axial compression is the main deformation mode, which resulted in high strength, stiffness, and buckling of the struts during deformation, producing fluctuating stress–strain curves. Bending-dominated lattice structures, on the other hand, deform mainly by bending the struts around the nodes, and they have lower mechanical properties and smoother stress–strain response [1, 16, 17].

Depending on their topology, the lattice structures are classified as strut based, which are formed by the interconnection of truss-like struts at the nodes, and triply periodic minimal surface lattice structures, which are mathematically generated periodic surfaces [1, 18, 19]. Numerous strut-based lattice structures were investigated and reported in the literature, including body-centered cell (BCC), face-centered cell (FCC), rhombic, Kelvin, octet truss, and Pillar Octahedral (other name BCCZ) lattice structure topologies [2, 12, 13, 18, 20–28]. It was found that by increasing the diameter of the strut, which leads to a higher relative density of the lattice structure, their mechanical properties and energy absorption increase, but it is to the detriment of its mass. Increasing nodal connectivity, which is also an important factor contributing to the mechanical properties, increases the strength and stiffness of the lattice structure [25]. By comparing different topologies, it was shown that octet truss lattice structure deforming in stretch-dominated manner reveals the highest strength and stiffness compared to other strut-based lattices [18, 23]. Similar properties of high strength and stiffness were observed in FCCZ (FCC lattice structure with vertical struts) and BCCZ (also called Pillar Octahedral) lattice structures formed by the addition of the vertical strut to FCC and BCC cell structures [2, 26]. On the other hand, BCC, rhombic, and Kelvin topologies experiencing bending-dominated failure have lower mechanical properties and stable plateau range [20, 21, 29]. All the works above used a solid strut of constant diameter. However, it was found that by using hollow struts, it is possible to stabilize the stress fluctuations during the post-buckling of the stretch-dominated octet truss lattice structure, without a significant reduction in strength and elastic modulus. This increases energy absorption [24].

Triply periodic minimal surface (TPMS) lattice structures, on the other hand, do not have explicit nodes and struts, and their geometry changes gradually. They are formed from periodic minimal surfaces by adding thickness (sheet-based TPMS) or by enclosing the surfaces to form a strut-like structure (skeletal TPMS) [18]. Several TPMS

topologies both skeletal and sheet-based were studied previously including, diamond, gyroid, and Schwarz primitive lattice structures [18, 30–33]. It was found that sheet-based TPMS lattices have higher strength and stiffness compared to skeletal-based TPMS structures, and their mechanical properties can surpass those of the strut-based lattice structures [18].

Graded lattice structures in which some parameter variables change gradually have also been investigated experimentally and numerically. Bai et al. studied graded lattice structures in which the diameter and the cell height of BCC lattice varied with the length [20]. In work by Maskery et al., the diameter of the BCC lattice was progressively varied [34]. In both works, it was observed that graded lattice structures can produce a new deformation mode in which post-buckling stress–strain response have step-like incremental behavior with multiple plateaus increasing their value with strain. This was not encountered in simple BCC structures.

Recently, novel lattice structures formed by combining different cell topologies were proposed. These cells usually have dissimilar properties: one having stretch-dominated topology and the other bending-dominated topology. These novel cell structures which incorporated two dissimilar topologies within one single unit were analyzed previously. It was found that these hybrid lattice structures exhibit the average mechanical properties of their parent unit cell topologies [35–37]. Their stress and strain curves showed high strength (as in stretch-dominated lattice structures) and moderate fluctuations (as in bending-dominated phase). This deformation pattern leads to an increase in energy absorption.

Although the development of hybrid lattice structures formed by the incorporation of two dissimilar topologies within one single unit is progressing, to the authors' knowledge, multi-morphology lattice structures that are formed by combining different cell unit topologies in specific orders were not studied well. One such work was done by Lei et al. [38], who studied horizontal, vertical, and circular arrangements of BCC, FCC, BFCC, and BFVC cell structures. It was found that vertical arrangement results in the highest mechanical properties.

Although the research in additive manufactured lattice structures is currently popular, and many articles have been published on the study of the mechanical properties of strut and TPMS lattices, the development of the multi-morphology or hybrid lattice structures started only recently, and limited publications are currently available. Nonetheless, multi-morphology lattice structures have more control over the mechanical properties. By changing the arrangement or relative density of each topology (or phase), it is possible to achieve more diverse deformation behaviors and mechanical properties. This may lead to even further expansion of the

lattice structures in engineering fields. For this reason, it is important to perform a further investigation in this field. Thus, this paper focuses on the mechanical properties, deformation behavior, and energy absorption characteristics of hybrid lattice structures formed from stretch-dominated Pillar Octahedral and bending-dominated rhombic cells structured patterned in several arrangements within one lattice. The performance of the hybrid lattice structures was juxtaposed against their single-phase counterparts. Several strut diameters were analyzed as these parameters affect the relative densities of the lattices as well as the mechanical properties. The Gibson-Ashby models that are based on power regressions were used to predict the strength, elastic modulus, and energy absorption capabilities of one-phase and hybrid lattice structures.

## 2 Methodology

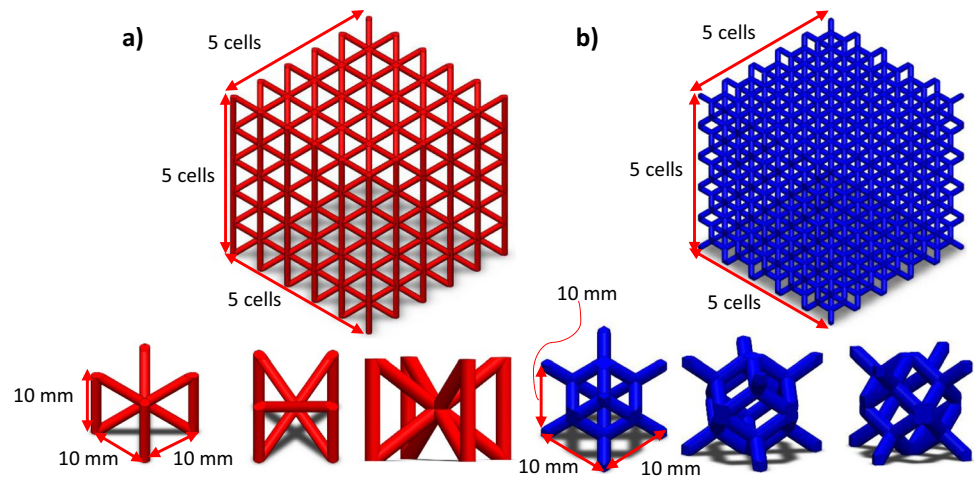
Both simple BCCZ and rhombic dodecahedron lattice structures, as well as their hybrids, were analyzed in this work. Hybrid lattice structures were formed by arranging cells of Pillar Octahedral (PO) and Rhombic Dodecahedron (RD) topologies in different orders. This section describes in detail the types of lattice structures, and their manufacturing and performance evaluation methodology.

### 2.1 Lattice structures

In this work, PO and RD cell structures were investigated. Their geometric topology is shown in Fig. 1. PO lattice (Fig. 1a) structure is classified as bending dominated according to Maxwell criterion. However, the addition of a strut along the loading direction increases its stiffness and strength significantly [39]. On the other hand, RD cell structure (Fig. 1b) is also bending-dominated according to Maxwell's criterion, and it has low stiffness and stable plateau stress region under compression [29]. Initially, the simple lattice structures were created as references to allow the comparison of their performance with that of the hybrid lattice structures. For this, cubic lattice structures with five cells along each direction were manufactured, and each cell has a size of 10 mm in all directions.

Figure 2 shows the arrangements of hybrid lattice structures that were considered. Figure 2a shows the simple PO lattice structure with red cubes corresponding to PO cells. Similarly, Fig. 2b represents the RD lattice structure with blue blocks designating RD cells. In the first hybrid pattern, RD and PO, cells are arranged in vertical periodic piles one after the other and formed hybrid vertical pile (HVP) arrangement shown in Fig. 2c. Similarly, RD and PO lattice structures were positioned in 2D chessboard order, and this pattern was propagated along the third direction, forming

**Fig. 1** Simple lattice structures. PO lattice structure (a) and RD lattice structure (b)



the Hybrid 2D Chess (HCh2D) lattice structure arrangement shown in Fig. 2d. Finally, when the chessboard order is preserved in three directions, a Hybrid 3D Chess arrangement is formed (HCh3D) as shown in Fig. 2e.

All lattice structures were studied with three different strut diameters of 1.5, 1.75, and 2 mm. Hence, overall, 15 different lattice structures were analyzed. For ease of interpretation, they received an alphanumeric designation consisting of the arrangement type and strut diameter. Table 1 summarizes the designations and corresponding strut diameter and relative density of each lattice. The last letter is a designation for strut diameter, where L, M, and H correspond to 1.5-, 1.75-, and 2-mm diameter respectively.

## 2.2 Lattice structure manufacturing and characterization

Lattice structures were manufactured using fused filament fabrication technology (FFF). Ultimaker S3 dual nozzle 3D printer was used for the fabrication. Lattices were produced from 2.85-mm Tough PLA plastic filament by its extrusion through the heated nozzle and deposition according to the sliced layer. To support overhanging features of the lattice structure, water-soluble supports made from PVA were used. Table 2 summarizes the manufacturing parameters used during the printing. On average, it took about 24 h to produce each part, and after the manufacturing, the parts were placed into water at 30 °C to dissolve the supports. Each lattice structure was manufactured two times to ensure the repeatability of compression tests.

After manufacturing the lattices and the removal of supports, quasi-static compression was performed. Liagong CM-50 universal testing machine with 100-mm compression platens and 50-kN load cell was used for the compression tests. Lattice structures were placed between the platens, and the compression tests were conducted with the strain rate of

0.667 s<sup>-1</sup>. A digital camera was placed in front of the testing machine to record failure modes of lattices. The frames were processed using the Python OpenCV computer vision module to compute the displacement of the platens.

Force  $F$  versus displacement  $\delta$  data was generated from the compression test, and it was converted to the stress  $\sigma$  versus strain  $\epsilon$  data by the following:

$$\sigma = \frac{F}{A} \quad (1)$$

$$\epsilon = \frac{\delta}{h} \quad (2)$$

where  $A$  and  $h$  are the initial area of the bounding box and height of lattice structure, respectively. Using the stress versus strain data the following data was obtained:

- Elastic modulus ( $E$ )
- Yield stress ( $\sigma_y$ )
- Yield strain ( $\epsilon_y$ )
- Plateau stress ( $\sigma_p$ )
- Densification strain ( $\epsilon_d$ )
- Volumetric energy absorption ( $\psi$ )
- Energy absorption efficiency ( $\eta$ )

The elastic modulus ( $E$ ), yield stress ( $\sigma_y$ ), and yield strain ( $\epsilon_y$ ) are found directly from the stress–strain curve. The elastic modulus was found as the slope of linear part of the stress–strain curve, while the yield stress and strain are defined as stress and strain that occur during the first peak on the curve. To find the volumetric energy absorption  $\psi(\epsilon_x)$  at some strain  $\epsilon_A$  the area under the stress–strain curve from zero to  $\epsilon_x$  needs to be obtained by using Eq. (3).

$$\psi(\epsilon_A) = \int_0^{\epsilon_A} \sigma(\epsilon) d\epsilon \quad (3)$$

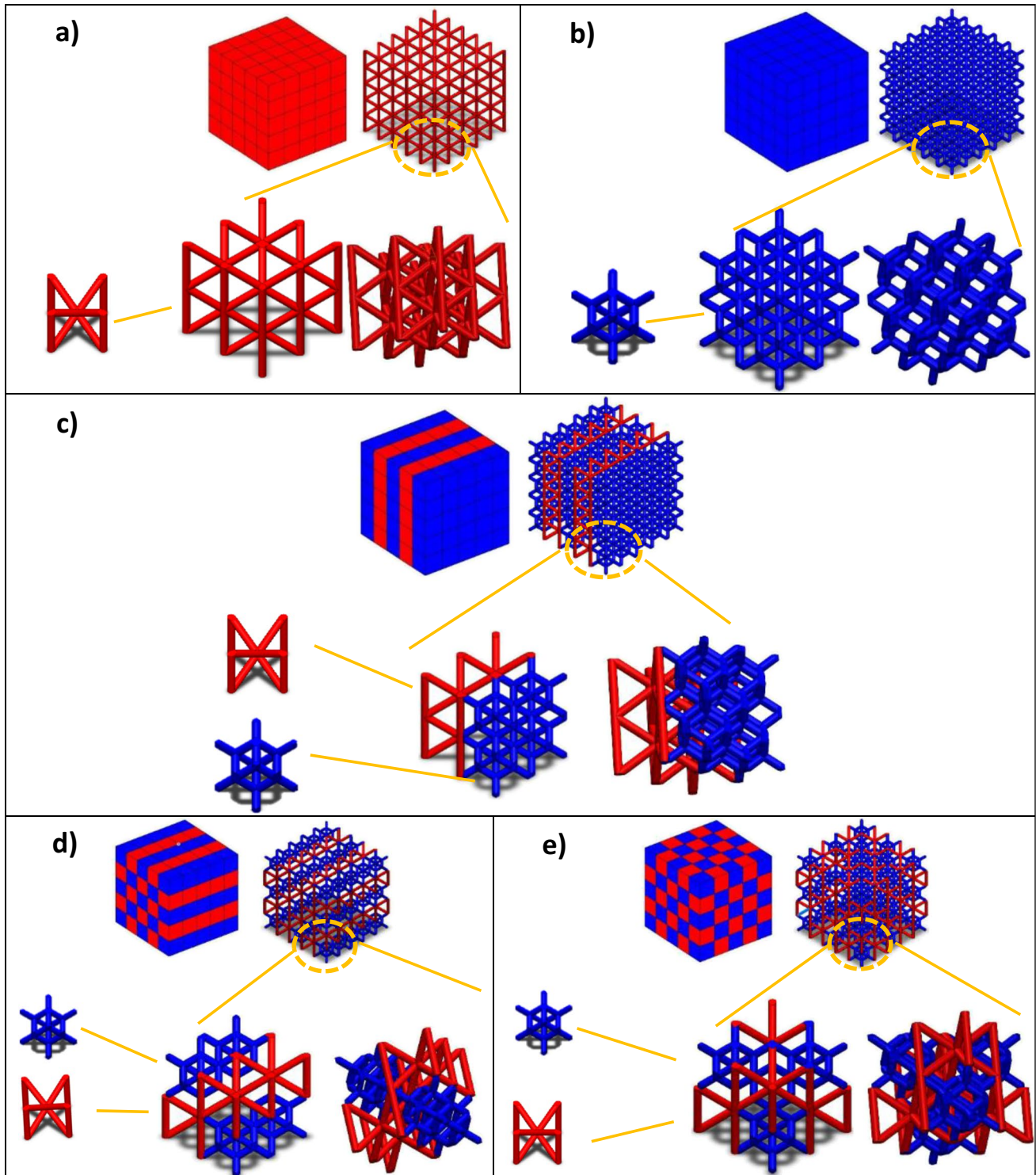


**Fig. 2** Lattice structures arrangements. (a) Simple PO. (b) Simple RD. (c) HVP. (d) HCh2D. (e) HCh3D. Red blocks correspond to PO cells, blue blocks designate RD cells

Lattices having larger relative density will experience higher stresses, and for this reason, their volumetric energy absorption will be larger. To compare lattices with different relative densities,

the specific energy absorption metric was generally adopted by the research community. This metric determines the energy absorption per unit of mass of the lattices and is given by the following:

**Table 1** Lattice structures designation

Lattice structure	Strut diameter (mm)	Nominal relative density
POL	1.5	0.1199
POM	1.75	0.1576
POH	2	0.1979
RL	1.5	0.1953
RM	1.75	0.2545
RH	2	0.3177
HVPL	1.5	0.1681
HVPM	1.75	0.2192
HVPH	2	0.2733
HCh2DL	1.5	0.1594
HCh2DM	1.75	0.2073
HCh2DH	2	0.2574
HCh3DL	1.5	0.1608
HCh3DM	1.75	0.2093
HCh3DH	2	0.2601

$$SEA(\epsilon_A) = \frac{\psi(\epsilon_A)}{\rho_c} \tag{4}$$

where  $\rho_c$  is the global density of the lattice structure given by the following:

$$\rho_c = \frac{\rho V_{lat}}{Ah} = \rho_{PLA} \left( \frac{\rho}{\rho_s} \right) \tag{5}$$

where  $\rho_{PLA}$  is the density of PLA material equal to 1220 kg/m<sup>3</sup> and  $V_{lat}$  is the volume occupied by lattice material and product  $A \times h$ —volume of the lattice bounding box.

In this study, the energy absorption quantities at the strain  $\epsilon_x = \epsilon_d$  were calculated, which is the densification strain. At this strain, the lattice structure is compressed to the point that it starts to behave as a solid material. The densification strain can be determined directly from the stress–strain curve as shown in Fig. 3 or it can be derived from the quantity

$$\eta_{@ \epsilon_d=1}(\epsilon_A) = \frac{\int_0^{\epsilon_A} \sigma(\epsilon) d\epsilon}{\max(\sigma_A) \times 1} \tag{6}$$

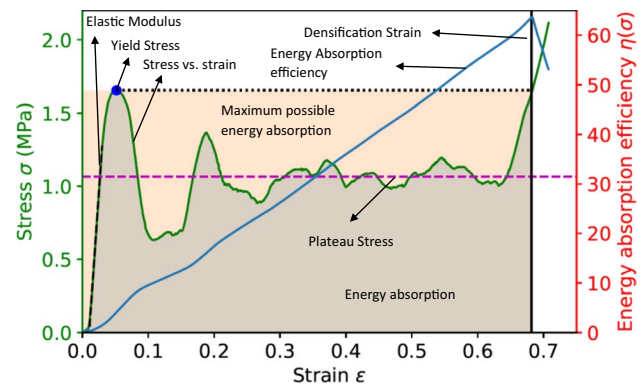


**Fig. 3** Typical stress–strain curve and summary of the performance metrics

which is the energy absorption efficiency at some strain  $\epsilon_A$  assuming that the lattice can be compressed to strain 1. According to Sun et al. [36], this metric increases and reaches its maximum level at the densification strain  $\epsilon_d$ , before starting to decline. Thus, the value of strain, at which the maximum value of this metric occurs is equal to densification strain. However, usually, lattices cannot be compressed to strain of 1, so the energy absorption efficiency given as the ratio of area under stress–strain curve and the area of the rectangle comprised by the peak stress and densification strain was used. The same approach to calculate the energy absorption efficiency was used in [40]. The energy absorption efficiency therefore is given by the following:

$$\eta = \frac{\int_0^{\epsilon_d} \sigma(\epsilon) d\epsilon}{\max(\sigma_d) \times \epsilon_d} \tag{7}$$

where  $\max(\sigma(\epsilon_d))$  is the maximum stress on the stress strain curve.

Finally, the plateau stress  $\sigma_p$  is given by the following:

$$\sigma_p = \frac{\int_{\epsilon_y}^{\epsilon_d} \sigma(\epsilon) d\epsilon}{\epsilon_d - \epsilon_y} \tag{8}$$

The force–displacement data was obtained from the compression tests, and a Python script was used to obtain the key mechanical properties according to Eqs. (1, 2, 3, 4, 5, 6, 7, and 8). Figure 3 shows the typical stress–strain and energy

**Table 2** Manufacturing parameters used in FFF

Infill percentage Tough PLA (%)	Infill percentage PVA (%)	Extrusion temperature Tough PLA (°C)	Extrusion temperature PVA (°C)	Bed temperature (°C)	Layer thickness (mm)	Nozzle diameter (mm)
100	20	215	225	60	0.2	0.4

absorption efficiency curves and summarizes the main performance characteristics used in the following study.

### 2.3 Mass properties

Before testing the mechanical properties of lattice structures, their masses were measured, recorded, and compared with their nominal masses. Table 3 shows the output. It can be seen that the measured masses of lattice structures are lower than their nominal counterparts. The maximum deviation from the weight of the nominal geometry is around 14%. This might be a process-related deficiency. In the fused filament fabrication process, due to the size of the nozzle, some places might not be filled up at 100% infill, and air gaps may also exist. As a result, these regions remain unfilled, leaving pores inside the material. Thus, the mass of the printed parts is lower than their nominal mass. Different printing setups (different nozzle sizes, speed of depositions) might lead to a different amount of porosity in the printed lattice structures, and the degree of their effect on the mechanical properties is unknown. For this reason, nominal mass was used to compute the specific mechanical properties in this work.

## 3 Results

Overall, 30 lattices were printed, and compression tests were performed to identify their average mechanical properties and energy absorption capabilities. Lattice structures were loaded up to the densification point, and tests were stopped manually when the densification stage occurred.

### 3.1 Stress–strain curves

After performing compressive tests, the force–displacement data was converted to stress–strain data by using Eqs. 1 and 2, and the result is shown in Fig. 4. The solid curves represent stress and strain profile while the “x” mark shows the yield stress of the lattice structure.

In Fig. 4, the experimental results were repetitive, and there is not much deviation in mechanical properties. All the curves have four distinctive regions. In the beginning, the compression platens deform surface irregularities that were introduced by FFF manufacturing technology, and for this reason, the small region with constant negligible stress appears at the beginning of the deformation process.

When surface irregularities are deformed, the whole lattice starts to experience loading and deformation. Initially, the elastic deformation with the stress proportional to strain is observed. After deformation passes the elastic region, the plastic region is observed, and the behavior of the lattice structure in that region strongly depends on the lattice patterning and strut diameter. Table 4 summarizes the values of the densification strain of lattice structures. As it can be seen, as the diameter of the strut and its relative density increases, the densification strain reduces.

Simple PO lattice structure has fluctuating stress and strain behavior in the plastic region. Furthermore, when the strut diameter is 1.5 mm, five peaks are observed corresponding to the collapse of five layers, however, when the diameter is 2 mm, a smoother response with three peaks is observed.

The deformation HVP topology resulted in different deformation behavior with distinctive first stress peaks

**Table 3** Measured and nominal masses of lattice structures

Lattice	Strut diameter (mm)	Sample 1 measured mass (g)	Sample 2 measured mass (g)	Average measured mass (g)	Nominal mass (g)	% of deviation of mass
POL	1.50	16.670	17.270	16.97	19.410	− 12.57
POM	1.75	21.530	22.990	22.26	25.700	− 13.39
POH	2.00	29.470	30.440	29.955	32.240	− 7.09
RL	1.50	26.010	26.960	26.485	29.780	− 11.06
RM	1.75	35.100	35.390	35.245	38.810	− 9.19
RH	2.00	43.060	45.760	44.41	48.450	− 8.34
VPL	1.50	22.550	23.870	23.21	26.403	− 12.09
VPM	1.75	31.160	30.140	30.65	34.563	− 11.32
VPH	2.00	38.600	39.190	38.895	43.349	− 10.27
HCh2DL	1.50	20.730	23.500	22.115	25.783	− 14.23
HCh2DM	1.75	29.330	30.550	29.94	33.800	− 11.42
HCh2DH	2.00	38.440	37.840	38.14	42.458	− 10.17
HCh3DL	1.50	24.060	22.220	23.14	26.022	− 11.07
HCh3DM	1.75	29.520	29.570	29.545	34.130	− 13.43
HCh3DH	2.00	38.230	40.110	39.17	42.894	− 8.68

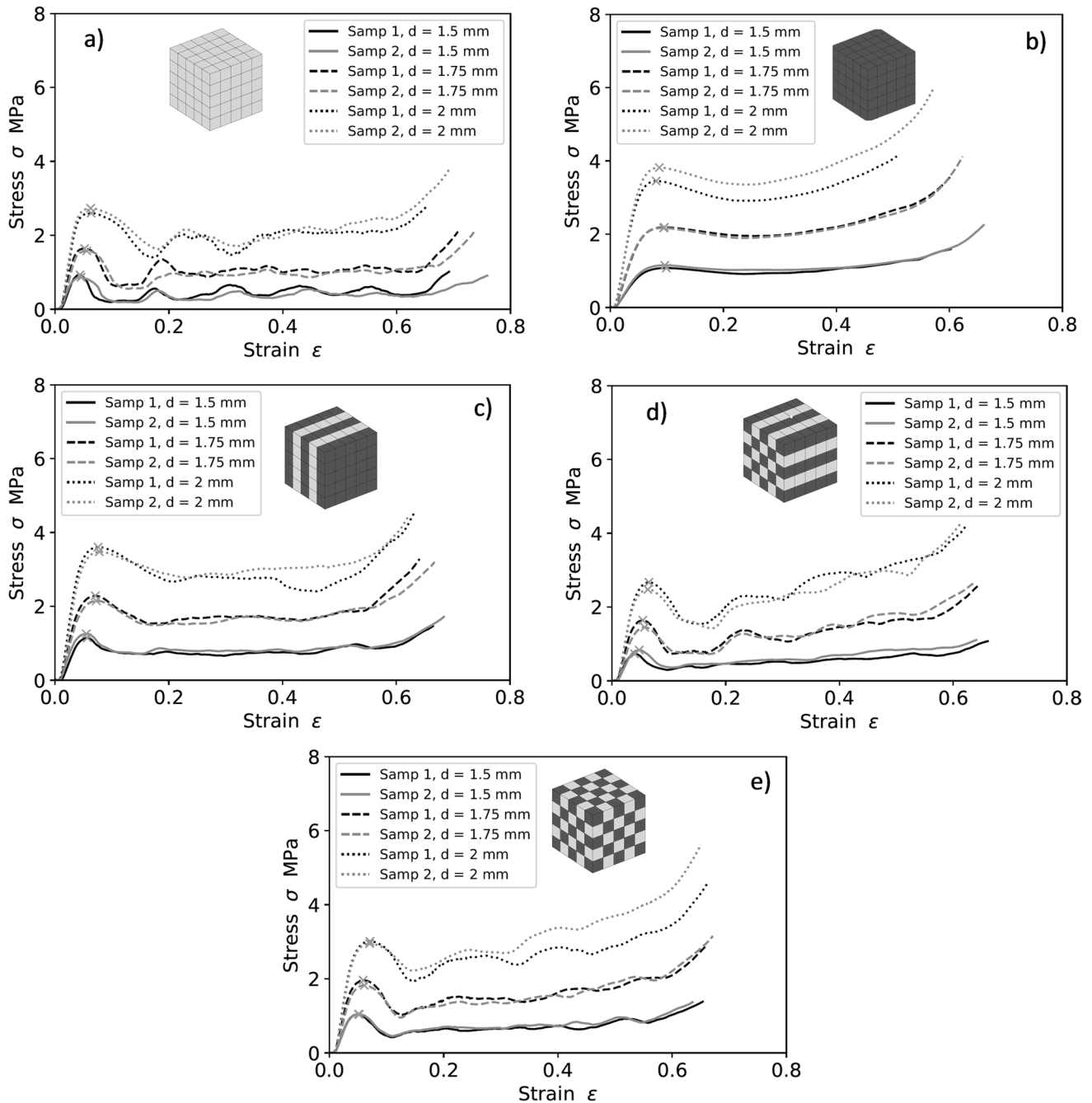


**Fig. 4** Stress versus strain curves of simple PO (a), simple RD (b), HVP (c), HCh2D (d), and HCh3D lattice structure patterns (e)

followed by its moderate drop and relatively stable behavior in the plastic region. Thus, combining the RD and PO lattice structures in a such pattern can lead to the combination of deformation behaviors of both lattice structures. On the other hand, the HCh2D and HCh3D topologies resulted in the most interesting stress and strain profile. After a sharp drop of stress, it starts to accumulate in the plastic deformation region, and the stress increases as the deformation progress. In the HCh2D pattern, this accumulation occurs

stepwise way: the stress increase, and plateau regions follow each other. It is interesting to note that such deformation behavior was also observed with graded BCC lattice structures in the previous works [20, 34].

Finally, after passing the plastic region, the lattice structures enter the densification stage. In this stage, the struts contact each other, and this leads to an increase in stress. The strain at which densification starts to occur depends on the strut diameter, and with its increase, the densification occurs earlier.

**Table 4** Densification strains of lattice structures

Lattice structure	Strut diameter (mm)	Nominal relative density	Densification strain
POL	1.50	0.120	0.718
POM	1.75	0.158	0.694
POH	2	0.198	0.634
RL	1.50	0.195	0.546
RM	1.75	0.255	0.538
RH	2	0.318	0.509
HVPL	1.50	0.168	0.633
HVPM	1.75	0.219	0.579
HVPH	2	0.273	0.574
HCh2DL	1.50	0.159	0.599
HCh2DM	1.75	0.207	0.555
HCh3DH	2	0.257	0.554
HCh3DL	1.50	0.161	0.595
HCh3DM	1.75	0.209	0.588
HCh3DH	2	0.260	0.587

### 3.2 Energy Absorption Characteristics

Volumetric energy absorption of the lattice structure was defined as the area under the stress versus strain curve as shown in Fig. 3 and Eq. 3. The resulting energy absorption versus strain plot is shown in Fig. 5. The energy absorption value increases with the increase of the strain. This follows directly from the definition of energy absorption, which is the area under stress versus strain curve, and the more the lattice deforms, the more energy it absorbs.

Table 5 summarizes key energy absorption performance matrices: maximum volumetric and specific energy absorption, specific energy, and its efficiency. The maximum volumetric energy absorption  $\psi(\epsilon_d)$  at densification strain  $\epsilon_d$  is shown in Fig. 6a. As it can be seen, the RD lattice structure has the highest value of volumetric energy absorption of 0.55, 1.09, and 1.67 MJ/m<sup>3</sup> when strut diameter is 1.5, 1.75, and 2 mm respectively. On the other hand, PO lattice structure results in the lowest value of volumetric energy absorption, which is equal to 0.31, 0.7, and 1.28 MJ/m<sup>3</sup> at 1.5-, 1.75- and 2-mm strut diameter, respectively. This is attributed to the differences in relative densities. RD topology has higher values of the relative density compared to the PO topology, and for this reason, its stress levels during the deformations are higher. Thus, the values of the energy absorption are also higher.

On the other hand, if the specific energy absorption values are compared as shown in Fig. 6b, the advantage of the RD topology seems less obvious due to higher mass. PO lattice topology, meanwhile, leads to one of the highest energy absorption values per unit of mass, which are equal to 2.12, 3.58, and 5.23 kJ/kg when strut diameter is 1.5, 1.75, and

2 mm respectively. Besides, the HVP topology also has large energy absorption per unit mass equal to 2.47, 3.62, and 4.94 kJ/kg. Values of the volumetric energy absorption show the dependence on both strut diameter and topology. With the increase in strut diameter, the energy absorption per unit volume increases as well. On the other hand, values of specific energy absorption are less dependent on the topology and depend mostly on the strut diameter.

Figure 7 represents energy absorption efficiency defined by Eq. 7. As it can be seen, the PO topology with the strut diameter of 1.5 mm has the lowest energy absorption efficiency of about 50%, while RD topology with the same strut diameter has much higher efficiency of about 80%. Hybrid lattice structures have energy absorption efficiencies just below of that of RD lattices. With the strut diameter of 1.5-mm HVP, HCh2D and HCh3D lattice structures have the efficiency of about 70%, which is 40% more compared to PO lattice. It is worth to mention that as the diameter of lattice structure increases, the effect of the lattice topology on its efficiency becomes negligible. With the strut diameter of 2 mm, all lattices have efficiency of 70–80%.

### 3.3 Mechanical properties

Absolute and specific mechanical properties such as yield stress, plateau stress, and elastic modulus of lattice structures were studied in the following work. Table 6 summarizes the key mechanical properties that were obtained during the experiments.

Figure 8 shows the absolute mechanical properties of lattices at diameters of 1.5, 1.75, and 2 mm. As the strut diameter increases, the mechanical properties of respective lattice structures increase as well. This occurs due to a rise in the relative density of lattice structures.

Similarly, mechanical properties also depend on the lattice structure type. The presence of uninterrupted vertical pillars in PO and HVP lattices leads to the highest elastic moduli among all structures investigated. On the other hand, the bending-dominated nature of RD topology results in the lowest value of elastic modulus. The elastic modulus of HCh2D and HCh3D topologies resulted in an average of that of PO and RD lattices. Similarly, when the specific elastic moduli of different lattice structures shown in Fig. 9 are compared, the PO lattice structure has the best performance due to its lower mass with elastic moduli equal to 1985, 2469, and 3012 MPa/kg at 1.5-, 1.75- and 2-mm strut diameter respectively. This is followed by HVP, HCh3D, and HCh2D, and RD topologies.

The plateau stress of the PO topology, on the other hand, has the lowest value of plateau stress equal to 0.43, 1.02, and 2.06 MPa when the diameter is equal to 1.5, 1.75, and 2 mm respectively. This occurs because of the fluctuating stress values in the plastic region, which reduces the plateau

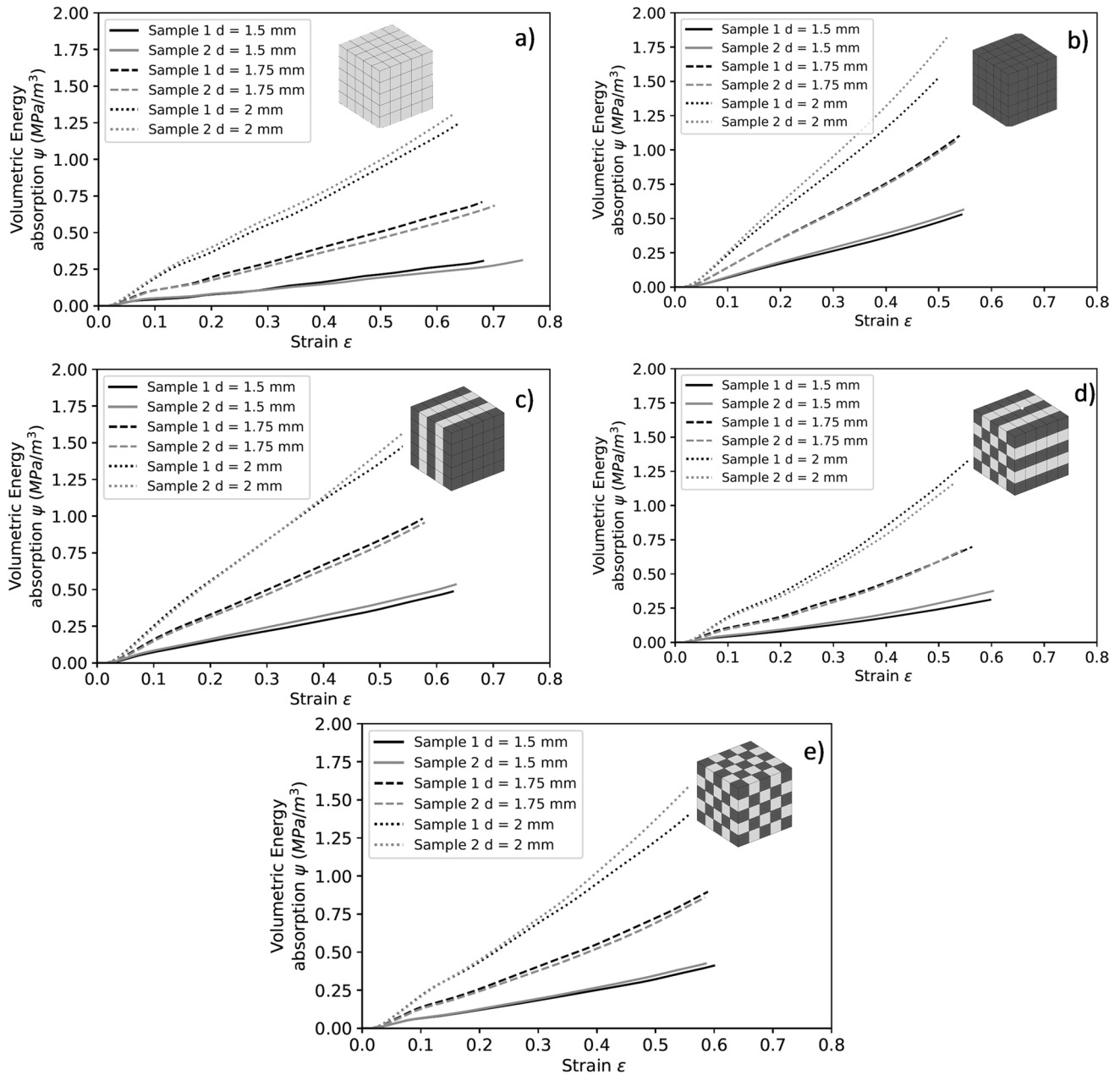


**Fig. 5** Energy absorption versus strain profile of simple PO (a), simple RD (b), HVP (c), HCh2D (d), and HCh3D lattice structure patterns (e)

stress. On the other hand, RD topology with a stable plastic region and higher relative density values at a given diameter has the highest values of plateau stress equal to 1.07, 2.16, and 3.5 MPa at 1.5-, 1.75-, and 2-mm diameter respectively. By combining these topologies, it is possible to obtain the averaged performance as in the case of HVP, HCh2D, and HCh3D topologies. A similar pattern is observed when specific mechanical properties are compared. However, the difference in the performance of different topologies is insignificant.

Finally, HVP lattice structures have the highest values of yield stress equal to 1.2, 2.22, and 3.54 MPa when strut diameter is 1.5, 1.75, and 2 mm respectively. This is slightly higher than the RD lattice structure with a yield stress of 1.11, 2.18, and 3.63 MPa at 1.5-, 1.75-, and 2-mm diameter strut respectively. This occurs due to the combined effect of uninterrupted vertical pillars and denser RD phase present in that topology. On the other hand, despite the presence of the vertical pillars, PO has lower values of the yield stress due to low relative density at a

**Table 5** Volumetric and specific energy absorption of lattice structures

Lattice structure	Strut diameter (mm)	Volumetric energy absorption (MJ/m <sup>3</sup> )	Specific energy absorption (kJ/kg)	Energy absorption efficiency (%)
POL	1.5	0.31	2.12	48.36
POM	1.75	0.7	3.58	62.83
POH	2	1.275	5.23	75.61
RL	1.5	0.547	2.24	75.83
RM	1.75	1.087	3.56	72.7
RH	2	1.673	4.29	73.94
HVPL	1.5	0.512	2.47	67.5
HVPM	1.75	0.972	3.62	75.83
HVPH	2	1.628	4.94	80.25
HCh2DL	1.5	0.34	1.74	69.28
HCh2DM	1.75	0.686	2.68	70.25
HCh3DH	2	1.28	4.04	71.67
HCh3DL	1.5	0.42	2.15	67.87
HCh3DM	1.75	0.879	3.43	73.13
HCh3DH	2	1.602	5.05	72.26

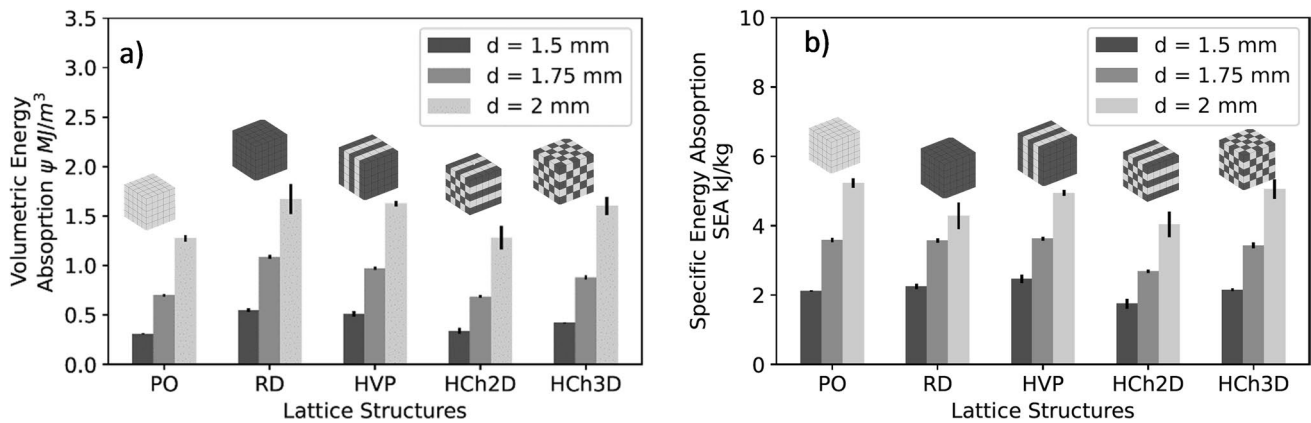


**Fig. 6** Volumetric energy absorption (a). Specific energy absorption of lattice structures (b)

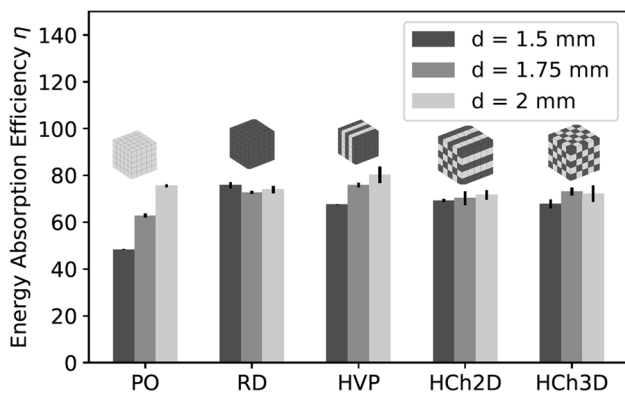


**Fig. 7** Energy absorption efficiency of lattice structures

given diameter, while HCh2D and HCh3D patterns show the averaged values. However, when specific yield stress is compared, PO and HVP lattice structures have the highest performance, while HCh2D topology results in the lowest values of specific yield stress.

As it was demonstrated, hybrid lattice structures result in the averaged performance of both lattice topologies. Thus, by controlling the relative density of each phase, it is possible to obtain tailored mechanical properties for the specific usage. For example, for shock absorption, to protect the body, it might be desired to have lower values of plateau stress, a stable stress–strain profile, and higher energy absorption characteristics. Hence, HCh3D topology might be a viable choice for this purpose.

**Table 6** Key mechanical properties of lattice structures

Lattice structure	Strut diameter (mm)	Yield stress (MPa)	Elastic modulus (MPa)	Plateau stress (MPa)	Specific yield stress (MPa/kg)	Specific elastic modulus (MPa/kg)	Specific plateau stress (MPa/kg)
POL	1.50	0.90	38.54	0.43	46.21	1986	22.29
POM	1.75	1.61	63.47	1.02	62.63	2469	39.81
POH	2	2.67	97.11	2.07	82.69	3012	64.09
RL	1.50	1.11	24.33	1.07	37.40	817	35.90
RM	1.75	2.18	48.74	2.16	56.12	1256	55.70
RH	2	3.63	88.32	3.51	75.00	1823	72.37
HVPL	1.50	1.20	42.08	0.83	45.48	1594	31.33
HVPM	1.75	2.22	68.83	1.74	64.19	1992	50.22
HVPH	2	3.54	108.34	2.95	81.70	2499	68.11
HCh2DL	1.50	0.78	31.48	0.59	30.34	1221	22.70
HCh2DM	1.75	1.55	55.89	1.28	45.76	1653	37.99
HCh3DH	2	2.57	84.13	2.42	60.61	1981	57.10
HCh3DL	1.50	1.04	40.34	0.72	40.03	1550	27.74
HCh3DM	1.75	1.89	66.30	1.55	55.48	1943	45.33
HCh3DH	2	2.98	95.04	2.87	69.53	2216	66.88

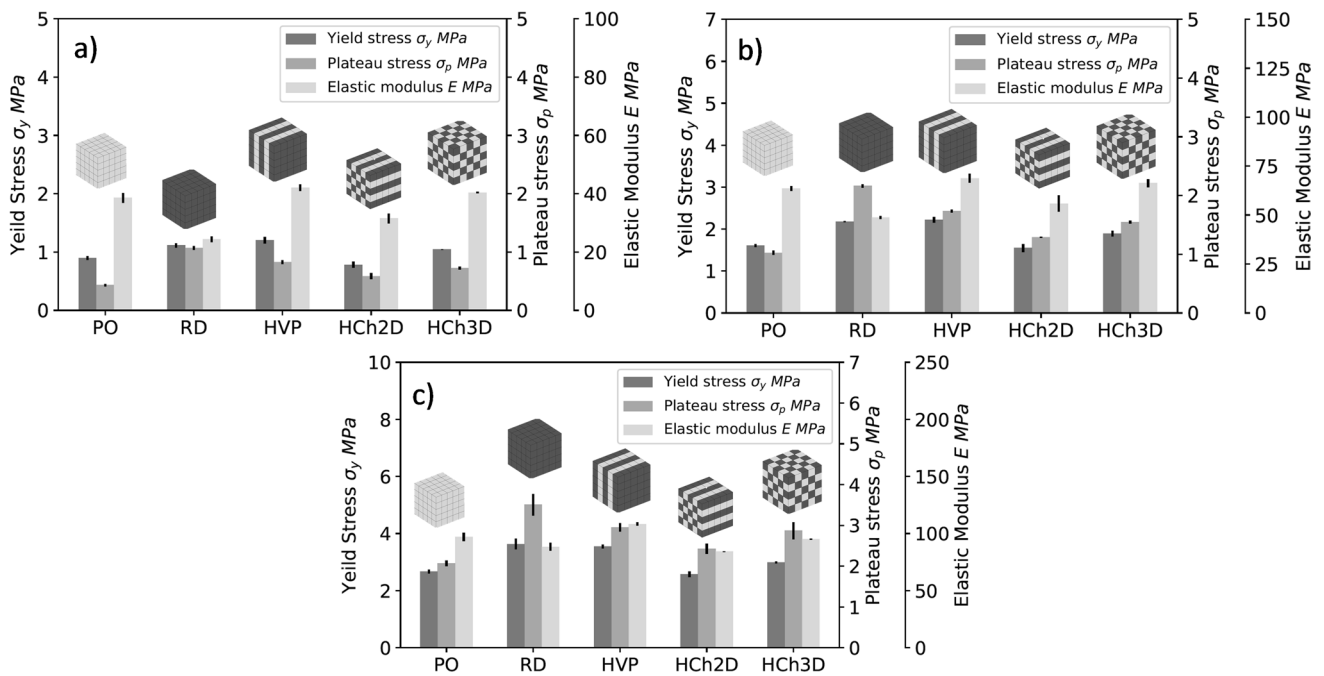


**Fig. 8** Yield stress, plateau stress, and elastic modulus of lattice structures with diameter of 1.5 mm (a), 1.75 mm (b), and 2 mm (c)

**3.4 Gibson and Ashby model**

To predict the yield stress and elastic modulus capabilities of lattice structures, the empirical relations based on Gibson and Ashby model [41] were established. According to this model, the mechanical properties are the power relations of the relative density, and thus

$$\frac{\sigma_y}{\sigma_{sy}} = C_1 \left( \frac{\rho}{\rho_s} \right)^{n_1} \tag{9}$$

$$\frac{E}{E_s} = C_2 \left( \frac{\rho}{\rho_s} \right)^{n_2} \tag{10}$$

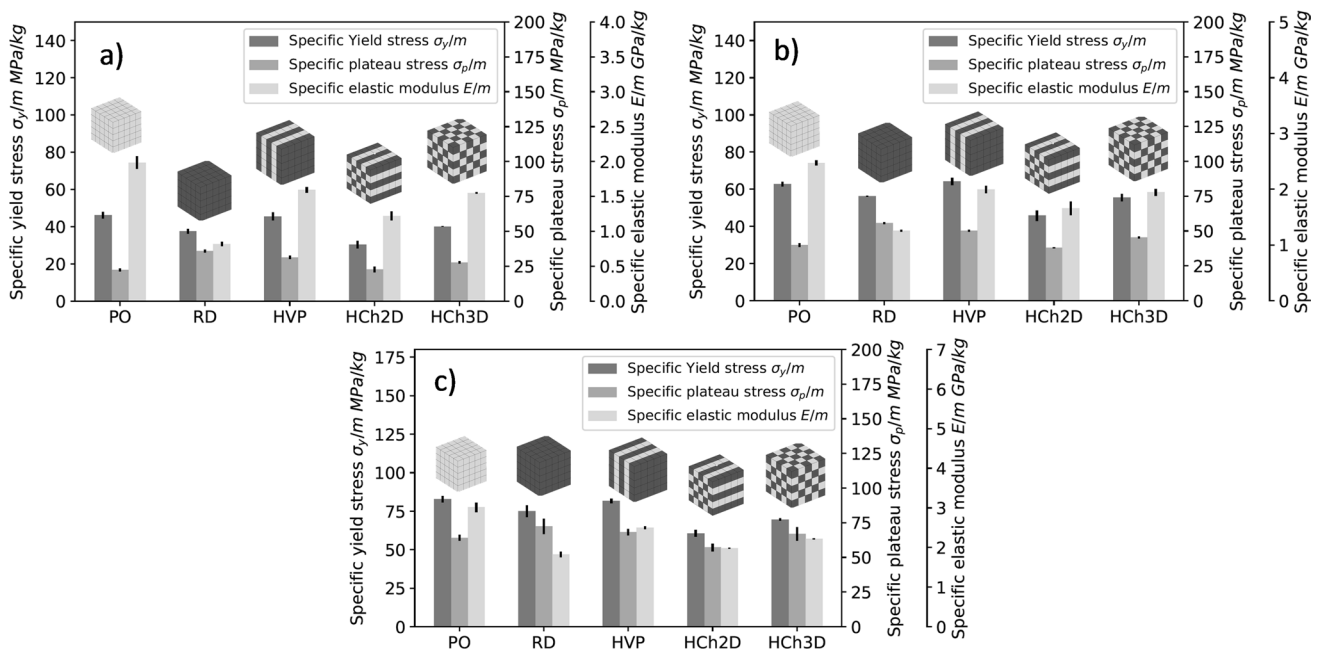


**Fig. 9** Specific yield stress, plateau stress, and elastic modulus of lattice structures with diameter of 1.5 mm (a) 1.75 mm, (b) and 2 mm (c)

The resultant mechanical properties are normalized for  $\sigma_{sy}$ ,  $E_s$  which are yield stress and elastic modulus of the parent Tough PLA material. Using this power regression relations, values of constants  $C_i$  and  $n_i$  for  $i=1,2$  were obtained for each lattice structure, and the result is shown in Figs. 10 and 11, respectively, and summarized in Table 7. All lattice structures follow the exponential regression model quite accurately with  $R^2$ —score close to 1. This shows that models are reliable at the given range of relative density and can be used for predictive purposes.

For simple PO lattice structure, the values of  $n_1$  and  $n_2$  are 2.19 and 1.85, respectively which shows that despite of the presence of vertical pillar structures, deformation mode is bending dominated. On the other hand, lattice structures produced from metal using powder-based techniques showed lesser values of these coefficients. For example, MacKown et al. [42] obtained values of  $n_1$  and  $n_2$  equal to 1.52 and 2.20 respectively, while Leary et al. [43] found these values to be 1.65 and 1.34, respectively. The difference might be attributed to the difference in manufacturing technology and materials used in this work. To the author’s knowledge, no previous works to investigate the Gibson and Ashby coefficients of BCCZ lattice structures were performed in the past. Hence, more works needs to be done to investigate this issue.

The RD lattice structure has the values of  $n_1$  and  $n_2$  exponents equal to 2.39 and 2.66 which is close to the findings of [44], who produced lattices from metal using electron beam melting and obtained values of  $n_1$  and  $n_2$  both equal to 2.2. Higher values of exponents show that mechanical properties of RD lattices are more dependent on the strut diameter than those of the PO structures. By forming a hybrid lattice

structures, it is possible to obtain values of  $n_1$  and  $n_2$  exponents equal to 2.19 and 1.98 for HVP, 2.44 and 2.00 for HCh2D, and 2.16 and 1.75 for HCh3D topologies.

### 4 Discussion

From Fig. 4, POL lattice structure experienced five peaks in the plastic zone corresponding to the failure of five layers of lattice structures. The buckling of vertical pillars of the PO topology is responsible for this fluctuating behavior [45]. This observation is corroborated by the video captures of the deformation mode associated with the lattice structure shown in Fig. 12. Because of the fluctuating behavior, the POL lattice structure cannot absorb deformation energy efficiently, and as the result, its efficiency is about 50%. The opposite is true for the rhombic dodecahedron lattice structures which have stable plastic stress zone as shown in Fig. 4, and as the result, their efficiency is about 80% at all strut diameters. A similar response of RD lattice was observed by [29].

Combining RD and PO lattice structures’ results in HVP, HCh2D, and HCh3D hybrid lattice structures. HVP lattice structures have a behavior, which is average to that of their parent lattices, with the relatively high specific yield stress of 45, 64, and 81 MPa/kg when strut diameter is 1.5, 1.75, and 2 mm, respectively, and stable plastic zone. From Fig. 10, it seems that the PO phase of the HVP lattice structure fails first by buckling the horizontal struts. After the failure of the PO phase, the load is transferred to the RD phase, and this does not cause a significant drop in stress. This results

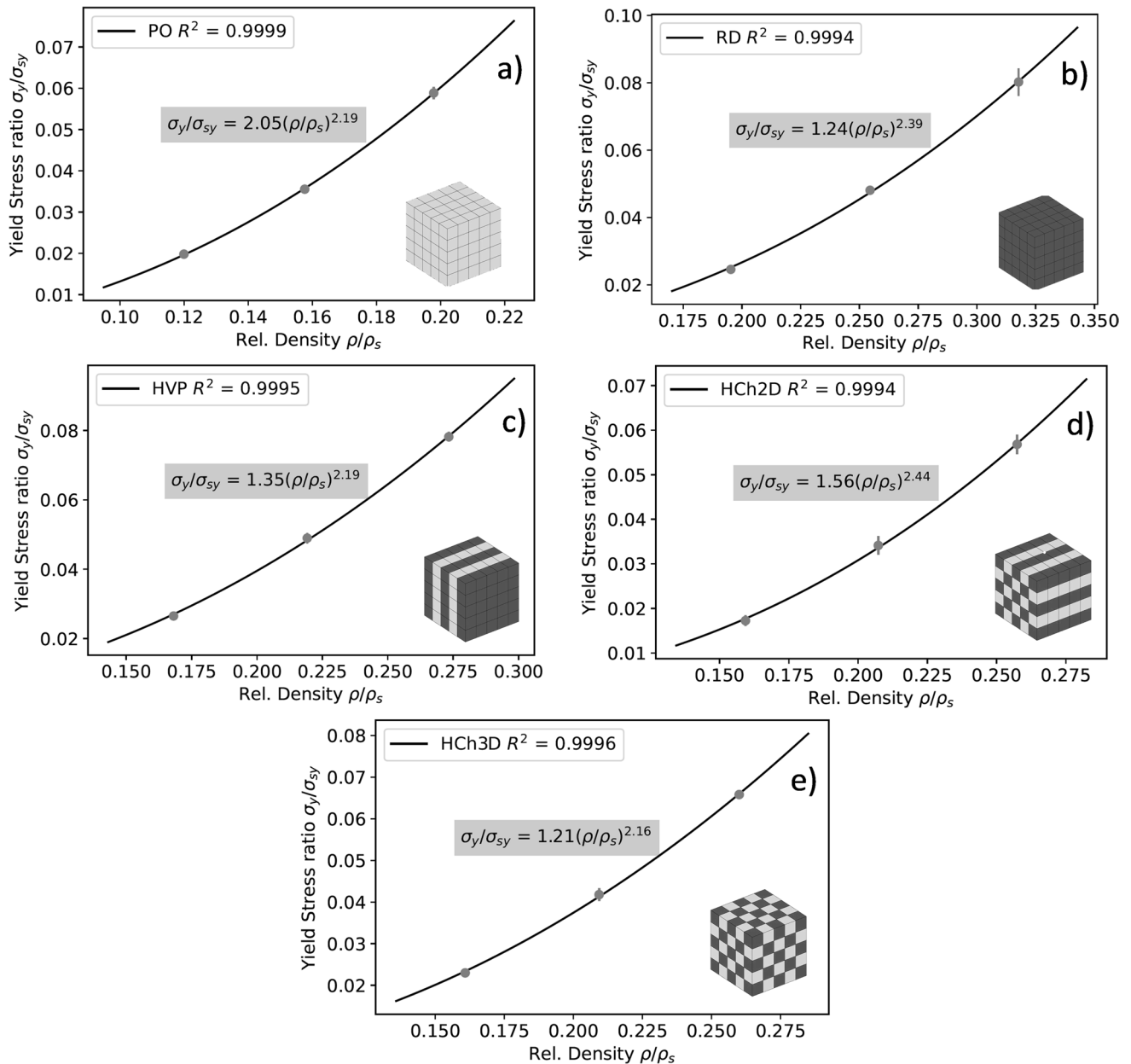


**Fig. 10** Exponential regression models for determining yield stress  $\frac{\sigma_y}{\sigma_{sy}}$  of PO (a), RD (b), HVP (c), HCh2D (d), and HCh3D (e)

in one of the highest specific energy absorptions of 2.5, 3.6, and 4.9 kJ/kg among the lattice structures investigated. Also, the absence of fluctuations in the plastic zone leads to the energy absorption efficiency of 70–80%.

With regards to the HCh2D and HCh3D lattice structures, when strain reaches 5–8%, both lattice structures fail by buckling the vertical struts, resulting in a stress drop as shown in Fig. 4. However, as the deformation progresses, the stress accumulates. The deformation mode of these structures is a failure by forming the shear bands as can be seen in Fig. 10. Due to the diagonal placement of the PO phase, the shear band failure progresses through this phase, while

the RD phase prevents the lattice from a drop in stress in a similar way as it was for the HVP lattice structure. As the result, the energy absorption efficiency of these lattice structures is also about 70–80%.

The effect of the strut diameter (relative density) on the mechanical performance of lattice structures is also significant. With the increase of the strut diameter, the plastic zone of the lattices during the compression is stabilized, and as the result, the energy absorption efficiency of the lattices increases with an increase in diameter.

The mechanical properties of lattice structures also increased with the rise in diameter. To compare the

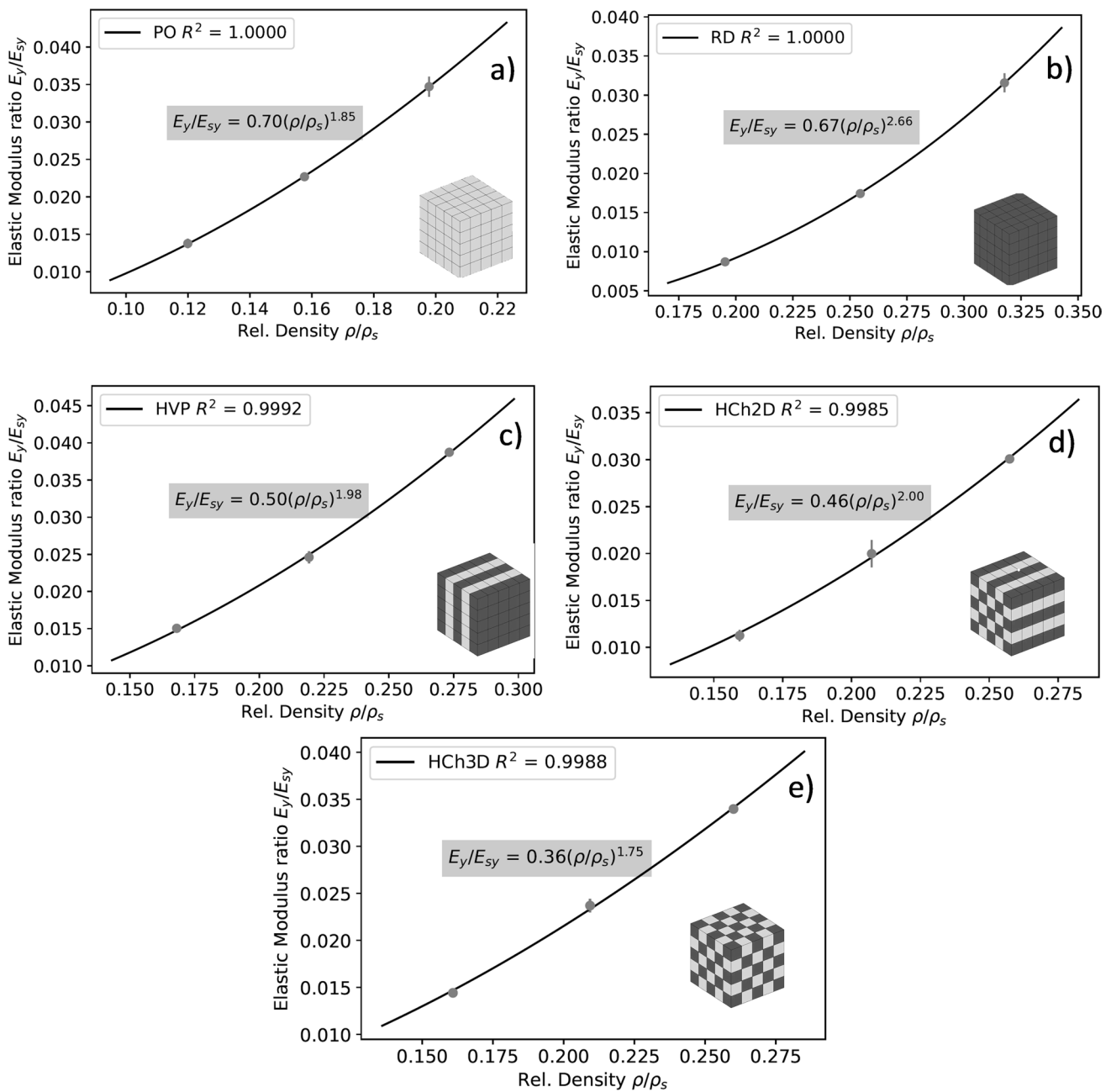


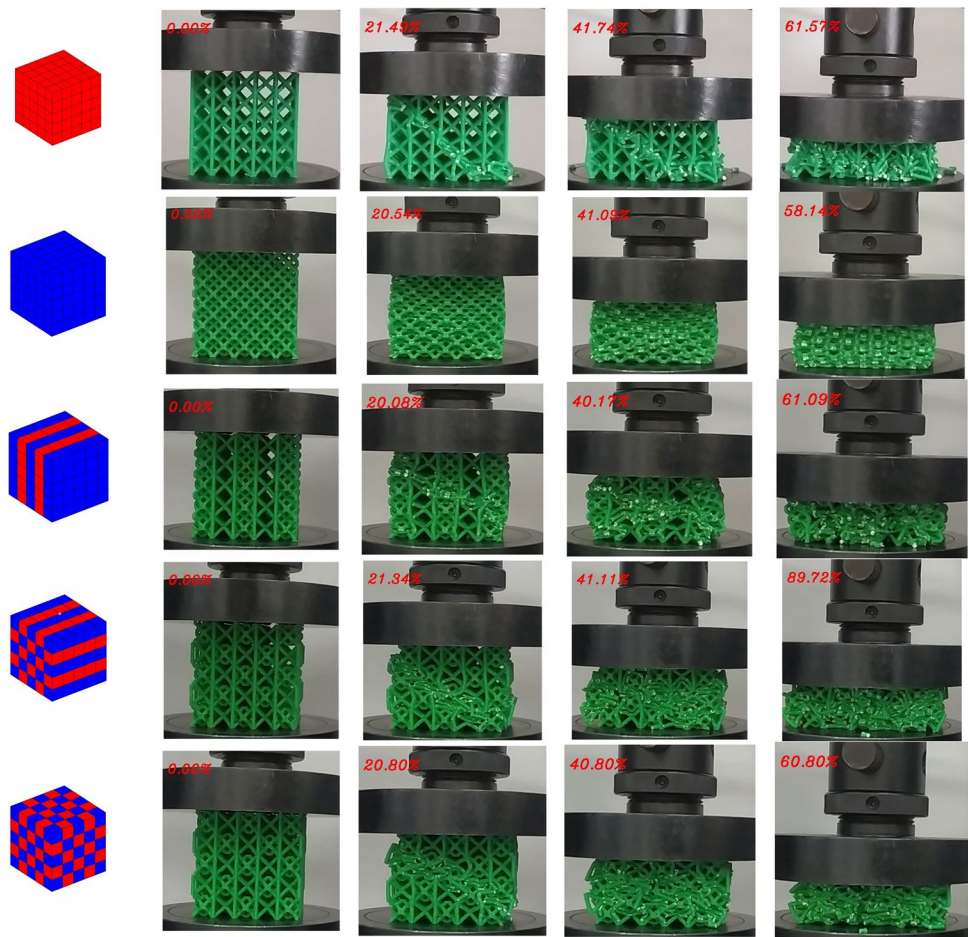
**Fig. 11** Exponential regression models for determining yield stress  $\frac{E_y}{E_{sy}}$  of PO (a), RD (b), HVP (c), HCh2D (d), and HCh3D (e)

**Table 7** Summary of the power regression coefficients

Lattice structure	$n_1$	$C_1$	$n_2$	$C_2$
PO	2.19	2.05	1.85	0.70
RD	2.39	1.24	2.66	0.67
HVP	2.19	1.35	1.98	0.50
HCh2D	2.44	1.56	2.00	0.46
HCh3D	2.16	1.21	1.75	0.36

mechanical performance of different lattice structures, the strength characteristics of each lattice structure were normalized with their respective masses, and the results are shown in Fig. 9. As it can be seen while the PO lattice structure has the highest elastic modulus and yield stress due to stiff vertical pillars, the fluctuating deformation behavior in the plastic zone causes the modest plateau strength. The opposite is true for the RD lattice structure, which deforms mostly by bending the struts. HVP lattice structure showed the averaged values of the mechanical

**Fig. 12** Deformation modes of lattice structures



properties, with relatively high modulus of elasticity, yield, and plateau stresses. However, as the diameter increases, the difference between specific mechanical properties of various lattice structures becomes less significant.

Comparing the mechanical properties and energy absorption capabilities of lattice structures, HVP lattices have the best performance among the lattices investigated. Their mechanical properties per unit of mass are comparable with those of the PO lattice structures, while the energy absorption characteristics are close to those of the RD lattices. Besides, they have stable plastic stress zone without repeating hardening–softening behavior similar to RD lattice structures, which leads to high plateau stress.

## 5 Conclusions

In this paper, an investigation of the mechanical performance and energy absorption characteristics of novel hybrid lattice structures formed from PO and RD cell structures was conducted. Three novel topologies were

proposed, and their elastic modulus, yield stress, plateau stress, and energy absorption characteristics for different strut diameters were investigated. It was found that PO lattice structures have the lowest absolute mechanical properties and volumetric energy absorption due to low relative density at a given diameter. Simple RD lattice structures, on the other hand, have one of the highest mechanical properties. However, when the specific mechanical properties are investigated, the PO has the highest values of specific elastic modulus and yield stress.

It was found that hybrid lattice structures have the average mechanical properties of pure lattice structures. HVP has high values of stiffness and yield stress equal to 1.2, 2.21, and 3.54 MPa and 42, 68.82, and 108.34 MPa at 1.5, 1.75, and 2 mm respectively. Despite this, the plastic range was relatively stable, which is a characteristic of the RD cell structure. HCh2D and HCh3D lattice structures have yield stress equal to 0.78, 1.54, 2.57, and 1.04, 1.89, and 2.98 MPa respectively for 1.5-, 1.75-, and 2-mm strut. Meanwhile, their elastic modulus was equal to 31.48, 55.89, 84.12, and 40.39, 66.29, and 95.04 MPa

respectively, for 1.5-, 1.75-, and 2-mm strut diameters. In the plastic range, they have accumulative stepwise stress versus strain behavior similar to that observed in the graded lattice structures. This behavior occurred most likely due to the dispersed RD phase which precluded the collapse of vertical pillars of PO lattice structures.

PO lattice structure has the lowest energy absorption efficiency of 50% when strut diameter is 1.5 mm due to fluctuations in the plastic deformation zone. On the other hand, RD lattice structures are most effective in energy absorption with efficiency of 80%. By combining these two types of lattice structures to form hybrid lattices, it is possible to achieve the energy absorption efficiency of 70–80%.

Finally, Gibson-Ashby power regression models were developed to predict the mechanical properties as the function of the strain. It was observed that the PO lattice structure had the lowest elastic modulus and yield stress exponents equal to 1.85 and 2.19, meaning that it is least dependent on the variation of relative density, while the RD lattice structure has the highest values equal to 2.66 and 2.39. Hybrid lattice structures have exponent values approximately lying in this range.

Future work might include the investigation of structure–property relationships of hybrid lattice structures, the investigation of their size effect, and the development of novel arrangements of the phases as well as their optimization using modern algorithms.

**Author contribution** All authors contributed to the study conception and design. Material preparation, data collection, and analysis were performed by Daniyar Syrlybayev, Asma Perveen, and Didier Talamona. The first draft of the manuscript was written by Daniyar Syrlybayev, and all authors commented on previous versions of the manuscript. All authors read and approved the final manuscript.

**Funding** This research was funded under the target program (No. OR07665556-OT-21) for the project entitled “Additive Manufacturing systems and metal powders for Kazakhstan industry”, by the Ministry of Industry and Infrastructure Development of the Republic of Kazakhstan.

**Data availability** The data presented in this study are available on request from the corresponding author.

**Code availability** The code presented in this study is available on request from the corresponding author.

## Declarations

**Ethics approval** Not applicable.

**Consent to participate** Not applicable.

**Consent for publication** Not applicable.

**Competing interests** The authors declare no competing interests.

**Open Access** This article is licensed under a Creative Commons Attribution 4.0 International License, which permits use, sharing, adaptation, distribution and reproduction in any medium or format, as long as you give appropriate credit to the original author(s) and the source, provide a link to the Creative Commons licence, and indicate if changes were made. The images or other third party material in this article are included in the article's Creative Commons licence, unless indicated otherwise in a credit line to the material. If material is not included in the article's Creative Commons licence and your intended use is not permitted by statutory regulation or exceeds the permitted use, you will need to obtain permission directly from the copyright holder. To view a copy of this licence, visit <http://creativecommons.org/licenses/by/4.0/>.

## References

1. Maconachie T et al (2019) SLM lattice structures: properties, performance, applications and challenges. *Mater Des* 183:108137
2. Gümriik R, Mines R, Karadeniz S (2013) Static mechanical behaviours of stainless steel micro-lattice structures under different loading conditions. *Mater Sci Eng, A* 586:392–406
3. Xiao Z et al (2018) Evaluation of topology-optimized lattice structures manufactured via selective laser melting. *Mater Des* 143:27–37
4. Abate KM, Nazir A, Jeng J-Y (2021) Design, optimization, and selective laser melting of vin tiles cellular structure-based hip implant. *Int J Adv Manuf Technol* 112(7):2037–2050
5. Bittredge O et al (2022) Fabrication and optimisation of Ti-6Al-4V lattice-structured total shoulder implants using laser additive manufacturing. *Mater* 15(9):3095
6. Dehghan-Manshadi A et al (2022) Additively manufactured Fe-35Mn-1Ag lattice structures for biomedical applications. *J Manuf Process* 80:642–650
7. Izri Z et al (2022) In silico evaluation of lattice designs for additively manufactured total hip implants. *Comput Biol Med* 144:105353
8. Tang H et al (2020) Tantalum bone implants printed by selective electron beam manufacturing (SEBM) and their clinical applications. *Jom* 72(3):1016–1021
9. Verma R et al (2022) Design and analysis of biomedical scaffolds using TPMS-based porous structures inspired from additive manufacturing. *Coatings* 12(6):839
10. Vasiliev V, Razin A (2006) Anisogrid composite lattice structures for spacecraft and aircraft applications. *Compos Struct* 76(1–2):182–189
11. Vasiliev VV, Barynin VA, Razin AF (2012) Anisogrid composite lattice structures—development and aerospace applications. *Compos Struct* 94(3):1117–1127
12. Boursier-Niutta C, Ciardiello R, Tridello A (2022) Experimental and numerical investigation of a lattice structure for energy absorption: application to the design of an automotive crash absorber. *Polymers* 14(6):1116
13. Dong G et al (2020) Design and optimization of solid lattice hybrid structures fabricated by additive manufacturing. *Addit Manuf* 33:101116
14. Richard CT, Kwok T-H (2021) Analysis and design of lattice structures for rapid-investment casting. *Mater* 14(17):4867
15. Wong KV, Hernandez A (2012) A review of additive manufacturing. *Int Sch Res Not* 2012:1
16. Hanks B et al (2020) Mechanical properties of additively manufactured metal lattice structures: data review and design interface. *Addit Manuf* 35:101301

17. Tamburrino F, Graziosi S, and Bordegoni M (2018) The design process of additively manufactured mesoscale lattice structures: a review. *J Comput Inf Sci Eng* 18(4). <https://doi.org/10.1115/1.4040131>
18. Al-Ketan O, Rowshan R, Al-Rub RKA (2018) Topology-mechanical property relationship of 3D printed strut, skeletal, and sheet based periodic metallic cellular materials. *Addit Manuf* 19:167–183
19. Xu Z et al (2021) Quasi-static behavior of 3D printed lattice structures of various scales. *Proc Struct Integr* 33:578–585
20. Bai L et al (2020) Mechanical properties and energy absorption capabilities of functionally graded lattice structures: experiments and simulations. *Int J Mech Sci* 182:105735
21. Bai L et al (2022) Heterogeneous compressive responses of additively manufactured Ti-6Al-4V lattice structures by varying geometric parameters of cells. *Int J Mech Sci* 214:106922
22. Bertocco A et al (2022) Lattice structures in stainless steel 17-4PH manufactured via selective laser melting (SLM) process: dimensional accuracy, satellites formation, compressive response and printing parameters optimization. *Int J Adv Manuf Technol* 120(7):4935–4949
23. Della Ripa M et al (2021) Numerical modelling of the mechanical response of lattice structures produced through AM. *Proc Struct Integr* 33:714–723
24. Intrigila C, Nodargi NA, Bisegna P (2022) The compressive response of additively-manufactured hollow truss lattices: an experimental investigation. *Int J Adv Manuf Technol* 120(5):3529–3541
25. Li C et al (2020) Architecture design of periodic truss-lattice cells for additive manufacturing. *Addit Manuf* 34:101172
26. Mazur M et al (2016) Deformation and failure behaviour of Ti-6Al-4V lattice structures manufactured by selective laser melting (SLM). *Int J Adv Manuf Technol* 84(5):1391–1411
27. Sadeghzade M, Gharehbaghi H, Farrokhbadi A (2021) Experimental and analytical studies of mechanical properties of additively manufactured lattice structure based on octagonal bipyramid cubic unit cell. *Addit Manuf* 48:102403
28. Sing SL, Wiria FE, Yeong WY (2018) Selective laser melting of lattice structures: a statistical approach to manufacturability and mechanical behavior. *Robot Comput-Integr Manuf* 49:170–180
29. Saremian R et al (2021) Experimental and numerical investigation on lattice structures fabricated by selective laser melting process under quasi-static and dynamic loadings. *Int J Adv Manuf Technol* 112(9):2815–2836
30. Al-Ketan O et al (2020) Functionally graded and multi-morphology sheet TPMS lattices: design, manufacturing, and mechanical properties. *J Mech Behav Biomed Mater* 102:103520
31. Al-Ketan O et al (2018) Microarchitected stretching-dominated mechanical metamaterials with minimal surface topologies. *Adv Eng Mater* 20(9):1800029
32. Guo X et al (2022) Enhancement in the mechanical behaviour of a Schwarz Primitive periodic minimal surface lattice structure design. *Int J Mech Sci* 216:106977
33. Maconachie T et al (2020) The compressive behaviour of ABS gyroid lattice structures manufactured by fused deposition modelling. *Int J Adv Manuf Technol* 107(11):4449–4467
34. Maskery I et al (2016) A mechanical property evaluation of graded density Al-Si10-Mg lattice structures manufactured by selective laser melting. *Mater Sci Eng, A* 670:264–274
35. Sun Z, Guo Y, Shim V (2021) Deformation and energy absorption characteristics of additively-manufactured polymeric lattice structures—effects of cell topology and material anisotropy. *Thin-Walled Struct* 169:108420
36. Sun Z, Guo Y, Shim V (2021) Characterisation and modeling of additively-manufactured polymeric hybrid lattice structures for energy absorption. *Int J Mech Sci* 191:106101
37. Xiao L et al (2022) Compressive performance and energy absorption of additively manufactured metallic hybrid lattice structures. *Int J Mech Sci* 219:107093
38. Lei H et al (2021) Deformation behavior of heterogeneous multi-morphology lattice core hybrid structures. *Addit Manuf* 37:101674
39. Leary M et al (2016) Selective laser melting (SLM) of AlSi12Mg lattice structures. *Mater Des* 98:344–357
40. Xinwei L (2020) Additively manufactured lightweight steel structures. Thesis, NUS. <https://scholarbank.nus.edu.sg/handle/10635/183961>
41. Gibson LJ (2003) Cellular solids. *MRS Bull* 28(4):270–274
42. McKown S et al (2008) The quasi-static and blast loading response of lattice structures. *Int J Impact Eng* 35(8):795–810
43. Leary M et al (2018) Inconel 625 lattice structures manufactured by selective laser melting (SLM): mechanical properties, deformation and failure modes. *Mater Des* 157:179–199
44. Li S et al (2014) Influence of cell shape on mechanical properties of Ti-6Al-4V meshes fabricated by electron beam melting method. *Acta Biomater* 10(10):4537–4547
45. Smith M, Guan Z, Cantwell W (2013) Finite element modelling of the compressive response of lattice structures manufactured using the selective laser melting technique. *Int J Mech Sci* 67:28–41

**Publisher's note** Springer Nature remains neutral with regard to jurisdictional claims in published maps and institutional affiliations.